

Calculations for the Pre-Calibration of LAMOST Active Optics

Yong Zhang^{1,2} and Xiang-Qun Cui¹

¹ National Astronomical Observatories / Nanjing Institute of Astronomical Optics & Technology, Chinese Academy of Sciences, Nanjing 210042; yzh@niaot.ac.cn

² Graduate School of the Chinese Academy of Sciences, Beijing 100039

Received 2004 August 9; accepted 2004 November 11

Abstract Large Sky Area Multi-Object Fibre Spectroscopic Telescope (LAMOST) is one of the major on-going national large scientific projects in China. Active optics is a key technology for the LAMOST with which the thin-mirror active optics and segmented-mirror active optics are tied in. A pre-calibration method considering all active forces and displacements specially for LAMOST has been developed in early 2004. We give a detailed mathematical derivation and calculation including numerical simulation and computer program realization of the pre-calibration method of LAMOST open-loop control for the third-order aspherical aberration. We have also carried out calculations on the application of the pre-calibration method and the parameters of actuator design in LAMOST active optics in observation mode, including estimations of the actuator ranges, the interval of active optics correction and the ranges and trends of load changes on all the actuators during LAMOST tracking a given star.

Key words: active optics — telescopes — instrumentation

1 INTRODUCTION

Active optics, including thin-mirror active optics and segmented-mirror active optics, is one of the most important key technologies for constructing modern large telescopes. Not only does it improve image quality by correcting some lower and even medium frequency errors, it also reduces substantially the cost of constructing telescopes. The Large Sky Area Multi-Object Spectroscopic Telescope (LAMOST) is the largest optical telescope under construction in China, involving with both thin and segmented-mirror active optics (Su & Cui 2002; Su et al. 1994; Su et al. 1998; Su et al. 2000; Wang et al. 1994; Wang et al. 1996; Wang 2003). It is a meridian reflecting ground-based Schmidt telescope with its optical axis fixed in the meridian plane. It realizes a breakthrough in combining large aperture with wide field of view in optical telescope by using original concepts and an ingenious design. One of its characteristics is its pioneering combination of both thin-mirror and two segmented-mirror technologies. It controls

not only the aspherical shape to correct errors such as spherical aberration of the primary mirror, gravitational and thermal deformation, but also the co-focus of all the segments of both the segmented primary mirror and the segmented Schmidt plate. During observation its main active correction mode is open loop control, but if it is needed for measuring the real-time actual systemic image quality, Shack-Hartmann wave-front sensor will be used to test systemically the image quality and the co-focus state for necessary correction. Su & Cui (2004) have developed a pre-calibration method for LAMOST open-loop correction. In the present paper we show some detailed realizations of the LAMOST pre-calibration method.

2 PRE-CALIBRATION METHOD IN LAMOST ACTIVE OPTICS

LAMOST active optics includes an open-loop correction and also an auxiliary close-loop correction, if necessary. In the close-loop correction, a Shack-Hartmann is used in wave front sensing (Zou & Zhang 2000; Zhang et al. 2004), the least square method (LSM) or the damped least square method (DLSM) is used to solve for all the actuator load corrective changes. While in actual open-loop tracking, to eliminate the third-order spherical aberration the aspherical shape of the reflecting Schmidt plate can be obtained by Wang et al. (1996) and Su & Cui (2004):

$$s = -\frac{1}{64f^3 \cos \theta} [(y_1^2 \cos^2 \theta + z_1^2)^2 - 2kr^2(y_1^2 \cos^2 \theta + z_1^2)] \quad , \quad (1)$$

where s is the aspheric depth on the Schmidt plate, a displacement from plane A, and tangent to Schmidt aspherical surface at point O_0 , to the surface s at point (y_1, z_1) (a right hand coordinate system, defined in Fig. 1, consists of the positive direction of s , O_0y_1 -axis and O_0z_1 -axis), θ is the incident angle of the ray, r the radius of the clear aperture and f the focal length. For LAMOST, f is equal to 20 000 mm, r 2000 mm and k 1.5, to obtain the minimum off-axis aberration. When LAMOST tracks a given star (declination δ , hour angle t) in its field of view (FOV) it is easy to obtain the incident angle θ and the rotating angle ψ between O_0y_1 -axis and O_0y_0 -axis in the Schmidt plate plane, and according to Eq. (1) the Schmidt plate shape can be easily obtained. Figure 2 shows the LAMOST Schmidt plate shape, when δ is equal to 40° , t 6° , θ 34.42° and Ψ 8.52° . This is a typical Schmidt plate aspherical shape. The shape for each segment can be divided from the Schmidt plate shape s . The correcting forces and displacements of all actuators of each segment in fig. 3 of Su & Cui (2004) can be obtained by the parallel calculations with LSM.

From the above analysis, in the open loop correction of real time active optics, the Schmidt plate will have to change its shape at short intervals to maintain a good image quality, because in different tracking position (δ, t) , the incident angle θ is different, the gravitational distortion and the surface s calculated by Eq. (1) are different too. The LAMOST Schmidt plate consists of 24 hexagonal segments. Obviously it is easy to correct the gravitational distortion, because the gravitational correcting forces have just a cosine relation of the Schmidt plate normal zenith distance Z :

$$f_G = G_S \cos Z \quad , \quad (2)$$

where f_G is the component vector of LAMOST segment gravity G_S on these forces actuators and G_S can be easily solved as counterforce by finite element analysis and it is constant and the same for all segments. So now the key issue is how to define which part of Schmidt plate a segment corresponds to and the timesaving solution for the forces and displacements. It is just what pre-calibration method does.

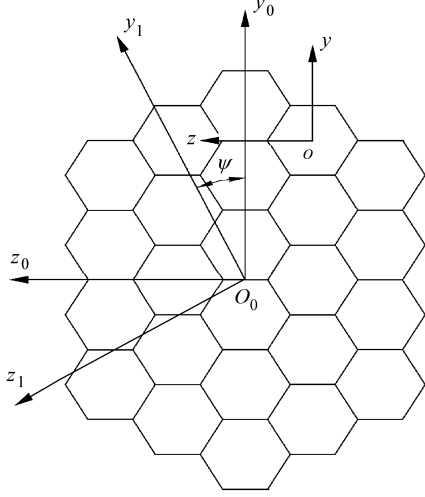


Fig. 1 Three coordinate systems of Schmidt plate.

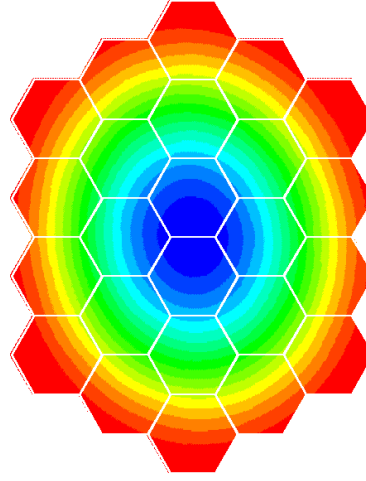


Fig. 2 Whole Schmidt plate shape to eliminate third-order spherical aberration calculated by formula (1) when $\delta = 40^\circ$, $t = 6^\circ$, $\theta = 34.42^\circ$ and $\Psi = 8.52^\circ$.

With the three coordinate systems shown in Fig. 1, position (y, z) can be changed into (y_0, z_0) of the coordinate $O_0Y_0Z_0$ from the local segment coordinate OYZ system by moving the separation (y_c, z_c) , which is the offset between these two coordinate system origins, O_0 and O . Here (y_c, z_c) represents the center of the LAMOST Schmidt plate segment containing the position (y, z) .

$$\begin{pmatrix} y_0 \\ z_0 \end{pmatrix} = \begin{pmatrix} y \\ z \end{pmatrix} + \begin{pmatrix} y_c \\ z_c \end{pmatrix}. \quad (3)$$

Then in the coordinate $O_0Y_1Z_1$ we can obtain (y_1, z_1) by rotating the coordinate system around the common origin O_0 , through an angle ψ :

$$\begin{pmatrix} y_1 \\ z_1 \end{pmatrix} = \begin{pmatrix} \cos \psi & \sin \psi \\ \sin \psi & -\cos \psi \end{pmatrix} \begin{pmatrix} y_0 \\ z_0 \end{pmatrix}. \quad (4)$$

We then express $y_1^2 \cos^2 \theta + z_1^2$ as a polynomial:

$$y_1^2 \cos^2 \theta + z_1^2 = b_1 + b_2 y + b_3 z + b_4 y^2 + b_5 z^2 + b_6 yz. \quad (5)$$

The six coefficients are :

$$b_1 = y_c^2 (\sin^2 \psi + \cos^2 \psi \cos^2 \theta) + z_c^2 (\cos^2 \psi + \sin^2 \psi \cos^2 \theta) - y_c z_c \sin 2\psi \sin^2 \theta,$$

$$b_2 = 2y_c \cos^2 \psi \cos^2 \theta + 2y_c \sin^2 \psi - z_c \sin 2\psi \sin^2 \theta,$$

$$b_3 = 2z_c \sin^2 \psi \cos^2 \theta + 2z_c \cos^2 \psi - y_c \sin 2\psi \sin^2 \theta,$$

$$b_4 = \cos^2 \psi \cos^2 \theta + \sin^2 \psi,$$

$$b_5 = \sin^2 \psi \cos^2 \theta + \cos^2 \psi,$$

$$b_6 = -\sin 2\psi \sin^2 \theta.$$

So, the aspherical surface s of each segment can be changed into the following polynomial of 15 terms with 15 coefficients:

$$s = a_1(y^4/factor) + a_2(y^3z/factor) + a_3(y^2z^2/factor) + a_4(yz^3/factor) + a_5(z^4/factor) \\ + a_6(y^3/factor) + a_7(y^2z/factor) + a_8(yz^2/factor) + a_9(z^3/factor) + a_{10}(y^2/factor) \\ + a_{11}(yz/factor) + a_{12}(z^2/factor) + a_{13}(y/factor) + a_{14}(z/factor) + a_{15}(1/factor), \quad (6)$$

$$s = a_1s_1 + a_2s_2 + a_3s_3 + a_4s_4 + a_5s_5 + a_6s_6 + a_7s_7 + a_8s_8 + a_9s_9 \\ + a_{10}s_{10} + a_{11}s_{11} + a_{12}s_{12} + a_{13}s_{13} + a_{14}s_{14} + a_{15}s_{15}. \quad (7)$$

The 15 terms and their coefficients are

$$a_1 = b_4^2/d, \quad a_2 = 2b_4b_6/d, \quad a_3 = (b_6^2 + 2b_4b_5)/d, \\ a_4 = 2b_5b_6/d, \quad a_5 = b_5^2/d, \quad a_6 = 2b_2b_4/d, \\ a_7 = (2b_2b_6 + 2b_3b_4)/d, \quad a_8 = (2b_2b_5 + 2b_3b_6)/d, \quad a_9 = 2b_3b_5/d, \\ a_{10} = (b_2^2 + 2b_1b_4 + cb_4)/d, \quad a_{11} = (2b_1b_6 + 2b_2b_3 + cb_6)/d, \quad a_{12} = (b_3^2 + 2b_1b_5 + cb_5)/d, \\ a_{13} = (2b_1b_2 + cb_2)/d, \quad a_{14} = (2b_1b_3 + cb_3)/d, \quad a_{15} = (b_1^2 + cb_1)/d, \quad (8)$$

$$c = -2kr^2, \quad d = \cos \theta, \quad factor = -64f^3,$$

$$s_1 = y^4/factor, \quad s_2 = y^3z/factor, \quad s_3 = y^2z^2/factor, \\ s_4 = yz^3/factor, \quad s_5 = z^4/factor, \quad s_6 = y^3/factor, \\ s_7 = y^2z/factor, \quad s_8 = yz^2/factor, \quad s_9 = y^3/factor, \\ s_{10} = y^2/factor, \quad s_{11} = yz/factor, \quad s_{12} = z^2/factor, \\ s_{13} = y/factor, \quad s_{14} = z/factor, \quad s_{15} = 1/factor. \quad (9)$$

We find that 15 s_i are the same for all the segments, and for different stars, different sets of 15 a_i can be calculated for each segment from the segmented shape s (i.e., see Fig. 2) by Eqs. (7) and (8).

After segment shapes are obtained, our aim is to acquire the actuator value l of each segment by LSM:

$$l = (C^T C)^{-1} C^T s. \quad (10)$$

In Eq. (10), C originates from discrete stiff matrix of the general LAMOST segment Finite Element Method (FEM) model and it is extended to include the influence of three displacement actuators (see Fig. 3). Here the positions of three displacements of a segment cell are the same as the three fixed support fulcrums of the segment, s is the discrete shape of the segment to be corrected. The sampling point number of the model is 3997, which is the length of the s vector. The vector l length is 37 including 34 force values and three displacement values. According to Eq. (7), l can be expressed in another form:

$$l = \sum_{i=1}^{15} a_i (C^T C)^{-1} C^T s_i = \sum_{i=1}^{15} a_i l_i, \quad (11)$$

where

$$l_i = (C^T C)^{-1} C^T s_i, \quad i = 1 \cdots 15. \quad (12)$$

Because all s_i are the same for the different segments, and also all l_i . We can calculate the above 15 l_i in advance and pre-store them in the computer. So, in the LAMOST open loop tracking, it is only necessary to calculate the 15 coefficients a_i of each segment, and then the l of all 24 segments (see Fig. 4) can be obtained easily by Eq. (11). This is one of advantage of the LAMOST pre-calibration method.

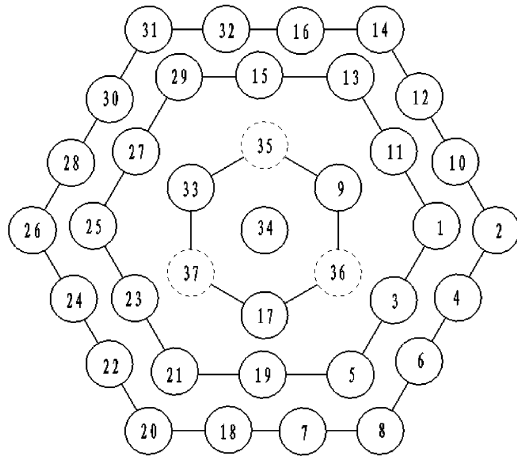


Fig. 3 Sequence number of all 37 actuators of segment. Forces actuators are listed from 1 to 34 and displacements actuators are from 35 to 37.

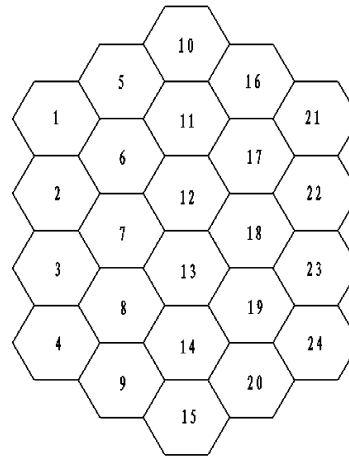


Fig. 4 Sequence number of all 24 segments of LAMOST Schmidt plate.

Table 1 Pre-calibration Coefficients while Tracking the Star
($\delta = 40^\circ$, $t = 6^\circ$, 6th segment)

Item Index	Corresponding Polynomial	Coefficients a_i
1	$s_1 (y^4)$	0.612183
2	$s_2 (y^3 z)$	-0.143395
3	$s_3 (y^2 z^2)$	1.70086
4	$s_4 (y z^3)$	-0.198217
5	$s_5 (z^4)$	1.16976
6	$s_6 (y^3)$	2.21443×10^3
7	$s_7 (y^2 z)$	2.39661×10^3
8	$s_8 (y z^2)$	2.74999×10^3
9	$s_9 (z^3)$	3.67138×10^3
10	$s_{10} (y^2)$	-6.06630×10^6
11	$s_{11} (y z)$	5.74867×10^6
12	$s_{12} (z^2)$	-8.27298×10^6
13	$s_{13} (y)$	-1.45936×10^{10}
14	$s_{14} (z)$	-1.75034×10^{10}
15	$s_{15} (1)$	-1.60596×10^{13}

Table 2 Pre-calibration Results and Final Results

Actuator Index	Pre-calibration Results l	Gravity Correction Results G_S	Final Results l_1
1	-28.240	19.692	-11.684
2	15.980	3.216	18.684
3	-16.892	18.814	-1.075
4	12.415	6.946	18.255
5	-26.795	19.742	-10.197
6	12.895	6.925	18.717
7	11.902	6.925	17.724
8	11.739	3.168	14.402
9	2.076	27.966	25.588
10	14.837	6.946	20.677
11	-18.410	18.814	-2.592
12	13.495	6.925	19.317
13	-17.557	19.742	-0.959
14	10.076	3.168	12.739
15	-5.316	18.814	10.502
16	6.010	6.925	11.833
17	1.377	27.966	24.890
18	10.437	6.946	16.277
19	-14.541	18.814	1.276
20	12.364	3.216	15.067
21	-20.354	19.692	-3.798
22	10.986	6.946	16.826
23	-11.803	18.814	4.014
24	9.708	6.925	15.530
25	-6.670	19.742	9.928
26	3.491	3.168	6.155
27	0.873	18.814	16.691
28	1.769	6.925	7.592
29	-4.131	19.692	12.425
30	2.267	6.946	8.107
31	0.210	3.216	2.913
32	5.590	6.946	11.430
33	-0.624	27.966	22.889
34	-2.359	25.331	18.938
35	37.961		37.961
36	22.535		22.535
37	35.532		35.532

3 RELIZATION AND EXAMPLES OF THE PRE-CALIBRATION METHOD

According to LAMOST pre-calibration method, the LAMOST pre-calibration realizations of the fifteen can be easily obtained.

The LAMOST working area is $-10^\circ \leq \delta \leq 90^\circ$ and $-11.25^\circ \leq t \leq 11.25^\circ$ (1.5 hours). For example, when we track a given star (δ equals to 40° , t equals to 6°) in brief we just simulate the sixth segment whose center (y_c, z_c) is (952.628 mm, 825.0 mm) in the global coordinate system $Y_0O_0Z_0$. So the incident angle is solved to be 32.42° , and the rotating angle ψ is 8.516° . Then the 15 coefficients a_i in Table 1 are calculated and the pre-calibration results are given in Table 2. By Finite Element Analysis gravity correction forces can be easily determined by Eq. (2). So the final actuator results can be obtained:

$$l_1 = l + f_G = l + G_S \cos(Z). \quad (13)$$

In the above example, the normal zenith distance Z of the Schmidt plate is 32.781 degrees.

The results of the above 37 pre-calibration actuators are compared with those calculated by the traditional fussy LSM calculation. In the latter, we should first divide the shape of correcting third-order aspherical aberration into two parts by fitting it with quasi-Zernike polynomials, then use the three displacement actuators to correct the piston and the tip/tilt, and use the 34 force actuators to correct the rest. With the existing computational and algorithmic capabilities, the absolute differences between the 37 actuator values calculated by the two methods are all less than 1×10^{-8} and the differences of the correcting remaining errors expressed as peak-to-valley (PTV) and root mean square (RMS) between the two methods are less than 1×10^{-10} micrometer and so can be considered as negligible and can be treated as only computational and algorithmic errors. This strongly verified an almost perfect agreement between the pre-calibration method and the traditional LSM method, and the correctness of the former. The results of pre-calibration of this segment are shown in Figs. 5 (Schmidt plate shape s), 6 (pre-calibration corrected shape s_C) and 7 (the pre-calibration remaining error $s - s_C$). It is noted that for the gravitation correction G_S , there exists an asymmetry due to the incomplete symmetry of node positions of the segment stiff matrix.

4 DISCUSSION AND CONCLUSIONS

With the pre-calibration method, many further tasks can be performed, such as estimating the actuator correction ranges, correcting the interval of active optics and concluding the ranges and trends of load changes on all the actuators during LAMOST tracking a given star.

4.1 Determination of Actuator Ranges

Before designing the actuators, it is very important to handle well the relation between the actuator range and the precision of applying the forces and displacements, which will dominate the correcting performance of LAMOST active optics. If the range is too wide, it will be difficult to maintain a high precision of applying forces, except using a more complicated and expensive mechanism. A wider actuator range means lower precision for the same quality-to-price ratio; on the other hand, if the chosen range is narrower than that of our minimum requirement, then the goal of good image quality from LAMOST active optics will not be realized. So, we should first make a good estimation of the actuator range, as a matter of great importance. Now by the pre-calibration we can easily calculate the exact ranges of all the actuators, not only for a single segment, for example, the sixth segment (see Fig. 8), but for all segments (see Fig. 9), to correct the third-order spherical error.

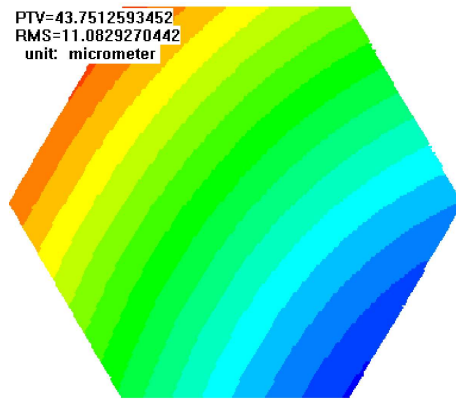


Fig. 5 Schmidt plate segment shapes ($\delta=40^\circ$, $t = 6^\circ$, $y_c = 952.627944$ mm, $z_c=825.0$ mm) including piston and tip/tilt. It is the same as the sixth segment shape in Fig. 2.

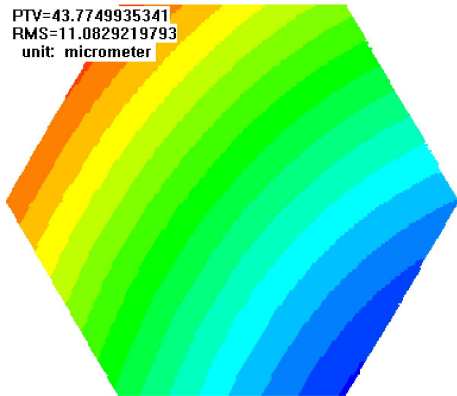


Fig. 6 Corrected shape including piston and tip/tilt after applying only pre-calibration results on 37-dimension stiff matrix.

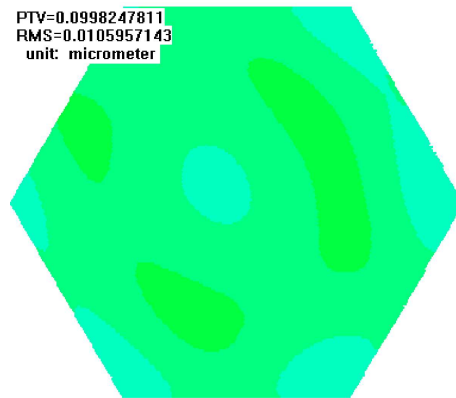


Fig. 7 Pre-calibration remaining error including piston and tip/tilt.

We can find that the actuator range for a single segment is much narrower than for all segments. As is known to all, an actuator is easy to design and to mechanically realize, if the actuator is always kept either in the positive force range or in the negative force range. That is to say, for a force actuator, we then only need a much simpler mechanism for either pushing one-way or pulling one-way. Obviously it is difficult to design different actuators for different segments. In addition, the final force actuator range should include gravitational correction forces. For uniformity, the final force actuator range, which corrects both open-loop three-order spherical aberration and gravitational deformation, is decided from Fig. 10 to satisfy the requirements of all segments and all actuators. There are four force actuators (9, 17, 33 and 34), which will never pass through the zero point. The relation between actuator values and hour angles tracking different stars with different declinations can be attained too. For example, when we use the sixth segment and a star of δ is 40° (see Figs. 11, 12, 13 and 14), during the

tracking the force range of all actuator changes monotonically (either increases monotonically or decreases monotonically), except when the telescope tracks the celestial pole (δ equals to 90°) or when the actuators are on a segment in the central column (segments indexed from 10 to 15) of the Schmidt plate through the meridian. When LAMOST tracks around the celestial pole neither the incident angle θ nor the Schmidt plate shape and the actuator values will vary. The force actuator values on every segment of the center column reach their minimum when the star approaches the meridian, and the values will increase when the star goes away from the meridian. Finally, the force actuator range changes from -43.680 to 61.521N , correcting only the third-order spherical error, and will be broadened to from -35.806 to 79.666N if the gravity correction is included. The displacement actuator range changes from 0.87 to 117.8 micrometer; if we do not consider the segment moving in the piston mode (the goal of LAMOST segmented mirror active optics is just to control co-focus, the segment moving in the piston mode need not be corrected, if it is small enough), then the range changes from -14.2 to 14.2 micrometer.

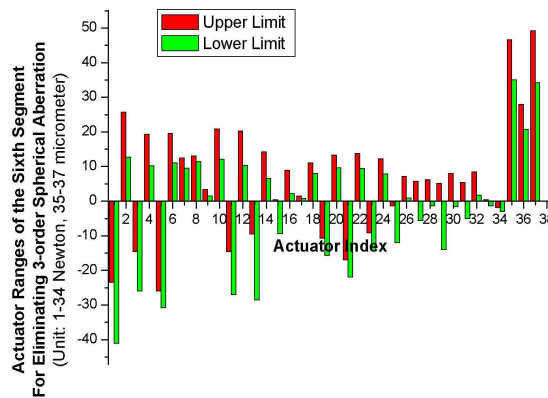


Fig. 8 All actuator ranges of the sixth segment for eliminating only 3-order spherical aberration (force actuator indexed from 1 to 34 and displacement actuators from 35 to 37).

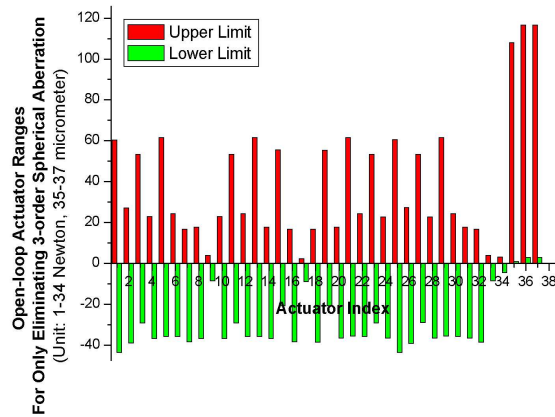


Fig. 9 All actuator ranges of all 24 segments for eliminating only 3-order spherical aberration (force actuator indexed from 1 to 34 and displacement actuators from 35 to 37).

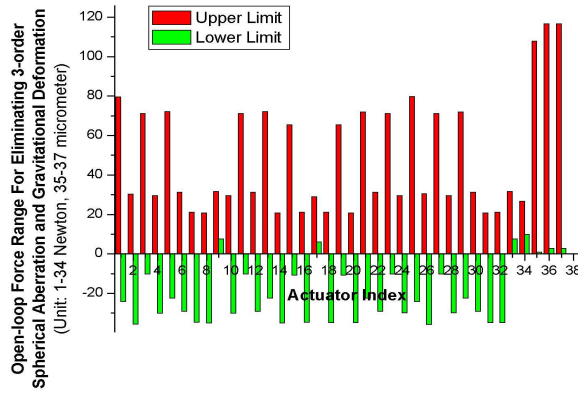


Fig. 10 All actuator ranges of all 24 segments for eliminating 3-order spherical aberration and gravitational deformation (force actuator indexed from 1 to 34 and displacement actuators from 35 to 37).

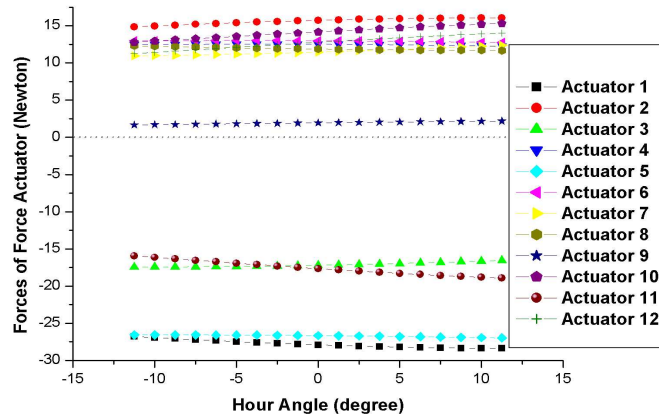


Fig. 11 Force actuator (from 1 to 12) value changes while tracking 1.5 hours athwart the meridian.

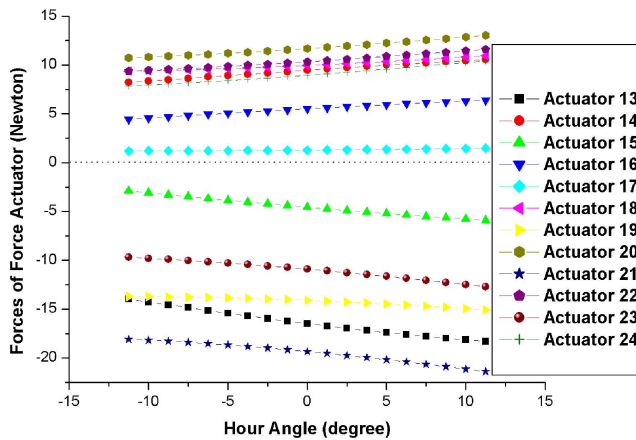


Fig. 12 Force actuator (from 13 to 24) value changes while tracking 1.5 hours athwart the meridian.

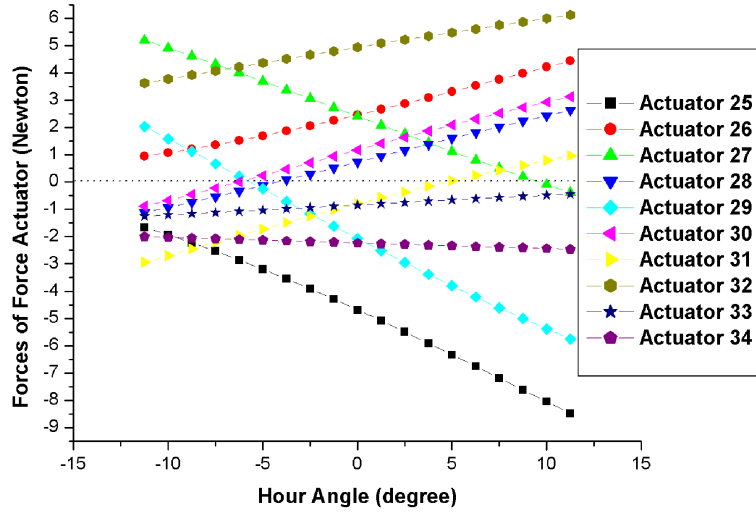


Fig. 13 Force actuator (from 25 to 34) value changes while tracking 1.5 hours athwart the meridian.

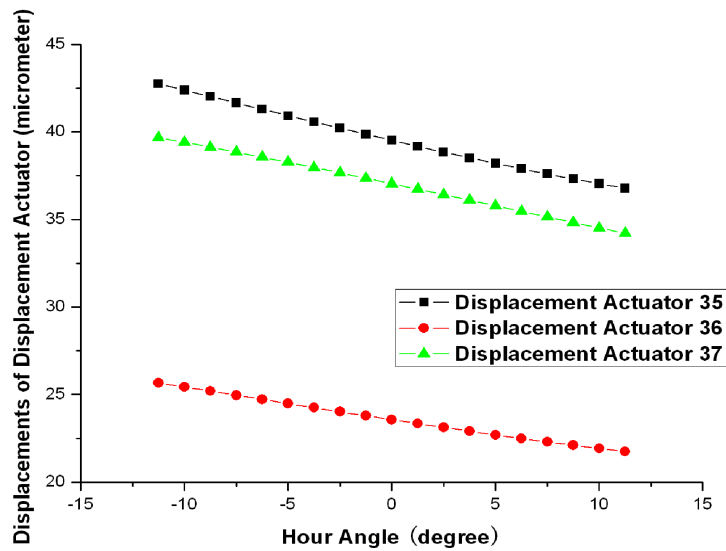


Fig. 14 Displacement actuator (from 35 to 37) value changes while tracking 1.5 hours athwart the meridian.

4.2 Estimation Of LAMOST Correction Interval

We can also make an estimation of the correction interval for LAMOST to maintain high image quality. From the LAMOST pre-calibration we know that the declination determines

not only the incident angle, but also the aspherical deformation calculated by Eq.(1) for a reflecting Schmidt plate. In the LAMOST working area ($-10^\circ \leq \delta \leq 90^\circ$), in fact the higher the declination is, the larger the incident angle, but the deformation of the Schmidt plate will not increase indefinitely. At 90 degrees declination, the aspherical figure is kept invariant, and there is no need to correct it endlessly after one open loop correction. For LAMOST the open-loop correction needs not to be kept continuously, rather, it can be made at intervals. Pre-calibration can help us to estimate the interval as a function of the declination. Here we use the image containing 80% of the energy, enclosed in 0.4 arcsec, as criterion for determining the correction interval. It is not of the Schmidt plate wavefront, but the projected wavefront of the plate on the plane. The wavefront is perpendicular to LAMOST prime optical axis at the position of the center O_0 of the spherical prime mirror, which is the same as the center of the Schmidt plate. The interval can be read from Fig. 15. At a declination of about 72.5 degrees, the correction interval reaches its minimum of about 2.81 minutes of time (0.7 degrees), and theoretically correction is not needed at declination 90 degrees (celestial pole). In addition, the criterion has an approximate linear correlation with the correction interval, i.e., if the criterion doubles (0.8 arcsec), the correction intervals will also double (5.62 minutes).

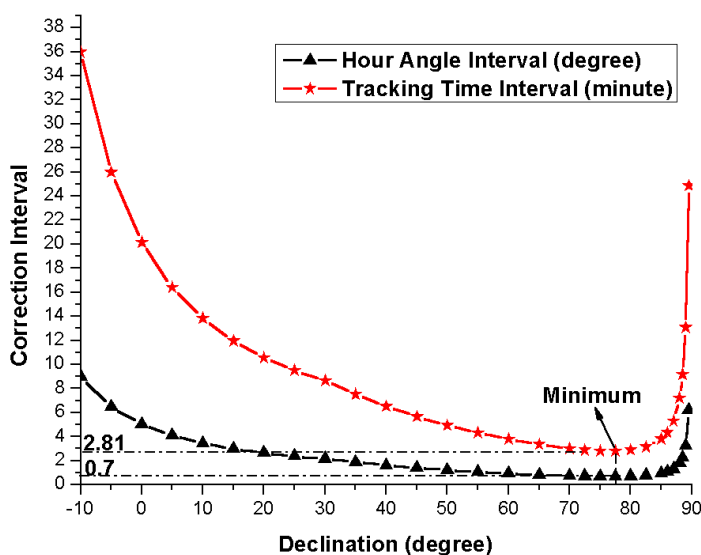


Fig. 15 Correction intervals using image diameter of 80% energy encircled in 0.4 arcsec.

4.3 Conclusions

In the above we have carried out some simulation calculations and applications of the LAMOST pre-calibration method. From all the analyses and results, several conclusions can be drawn.

Compared with other pre-calibration methods on circle mirror shape, the LAMOST pre-calibration makes a breakthrough to hexagonal mirror shape. The LAMOST pre-calibration method is highly accurate, and is different from other pre-calibration methods in active optics. Using Eq. (1) to calculate the Schmidt plate shape has an accuracy better than 0.02 arcsec.

The pre-calibration method gives a shortcut to LAMOST open-loop active correction. Because without the pre-calibration, we would need to calculate separately for as many as 34 forces and three displacements (involving many more steps the procedure). Now we just need to calculate no more than 15 coefficients a_i . After that, what we should do is only to use Eq. (11) to solve for the actuator values l with these coefficients, and to solve for the final actuator results l_1 by Eq. (13).

According to the analysis, we can make reasonable theoretical estimations on actuator ranges and correction intervals, which are essential for the design of the actuators. To correct the 3rd-order spherical aberration and segment gravity, the force actuator range is from -40N to 80N and the displacement range is from -15 to 15 micrometer. In practice, because of some unavoidable manufacture and installation errors, the range of force actuator will be broadened. Certainly the range of displacement actuator should be relaxed, because of segment cell gravity and truss thermal deformation. At least these ranges should be multiplied by a safety factor larger than 1, to be chosen by experience.

Acknowledgements We thank Prof. Su Ding-Qiang for his great care and very helpful, constructive advice.

References

- Su D. Q., Cui X. Q., 2004, *Chin. J. Astron. Astrophys.*, 4, 1
Su H. J., Cui X. Q., 2002, In: Jacobus M. Oschmann, L. M. Stepp, eds., *Proc. SPIE 4837, Conference on Large Ground-based Telescopes*, 26
Su D. Q., Jiang S. T., Zou W. Y., Yang S. M., Zhang H. Y., Zhu Q. C., 1994, In: L. M. Stepp, ed., *Proc. SPIE 2199, Conference on Advanced Technology Optical Telescopes V*, 609
Su D. Q., Cui X. Q., Wang Y. N., Yao Z. Q., 1998, In: L. M. Stepp, ed., *Proc. SPIE 3352, Conference on Advanced Technology Optical/IR Telescopes VI*, 76
Su D. Q., Zou W. Y., Zhang Z. C., Qu Y. G., Yang S. Y., Wang L. J., Rao Y. M., 2000, In: P. Dierickx, ed., *Proc. SPIE 4003, Conference on Optical Design, Materials, Fabrication, and Maintenance*, p.417
Wang S. G., 2003, *Chin. J. Astron. Astrophys.*, 3, 1
Wang S. G., Su D. Q., Hu Q. Q., 1994, In: L. M. Stepp, ed., *Proc. SPIE 2199, Conference on Advanced Technology Optical Telescopes V*, 341
Wang S. G., Su D. Q., Chu Y. Q., Cui X. Q., Wang Y. N., 1996, *Appl. Opt.*, 35, 5155
Zhang Y., Yang D. H., Cui X. Q., 2004, *Appl. Opt.*, 43, 729
Zou W. Y., Zhang Z. C., 2000, *Appl. Opt.*, 39, 250